Title

Genomic Complexity Profiling Reveals That HORMAD1 Overexpression Contributes to Homologous Recombination Deficiency in Triple-Negative Breast Cancers

Journal

Cancer Discovery, 5(5)

ISSN

2159-8274

Authors

Watkins, Johnathan
Weekes, Daniel
Shah, Vandna
et al.

Publication Date

2015-05-01

DOI

10.1158/2159-8290.cd-14-1092

Peer reviewed

HHS Public Access

Author manuscript

Cancer Discov. Author manuscript; available in PMC 2015 November 01.

Published in final edited form as:

Cancer Discov. 2015 May ; 5(5): 488–505. doi:10.1158/2159-8290.CD-14-1092.

Genomic complexity profiling reveals that HORMAD1 overexpression contributes to homologous recombination deficiency in triple-negative breast cancers

Johnathan Watkins[1,2,3,*], **Daniel Weekes**[1,3,*], **Vandna Shah**[1,3], **Patrycja Gazinska**[1,3], **Shalaka Joshi**[1,3], **Bhavna Sidhu**[1,3], **Cheryl Gillett**[3,4], **Sarah Pinder**[3,4], **Fabio Vanoli**[5], **Maria Jasin**[5], **Markus Mayrhofer**[6], **Anders Isaksson**[6], **Maggie C.U. Cheang**[7], **Hasan Mirza**[1,3], **Jessica Frankum**[8], **Christopher J. Lord**[8], **Alan Ashworth**[8,$], **Shaveta Vinayak**[9,#], **James M. Ford**[9], **Melinda L. Telli**[9], **Anita Grigoriadis**[1,3,*], and **Andrew N.J. Tutt**[1,3,8,*,§]

[1]The Breakthrough Breast Cancer Research Unit, King's College London, UK

[2]Institute for Mathematical and Molecular Biomedicine, King's College London, UK

[3]Department of Research Oncology, King's Health Partners AHSC, Life Sciences and Medicine, King's College London, UK

[4]King's Health Partners Cancer Biobank, King's College London, UK

[5]Developmental Biology Program, MSKCC, New York, NY 10065, USA

[6]Science for Life Laboratory, Department of Medical Sciences, Uppsala University, Uppsala, Sweden

[7]Clinical Trials and Statistics Unit (ICR-CTSU) at The Institute of Cancer Research, Surrey, UK

[8]The Breakthrough Breast Cancer Research Centre, The Institute of Cancer Research, London, UK

[9]Department of Medicine, Stanford University School of Medicine, Stanford, CA, USA

Abstract

Triple-negative breast cancers (TNBCs) are characterised by a wide spectrum of genomic alterations, some of which might be caused by defects in DNA repair processes such as homologous recombination (HR). Despite this understanding, associating particular patterns of genomic instability with response to therapy has been challenging. Here, we show that Allelic-imbalanced Copy Number Aberrations (AiCNA) are more prevalent in TNBCs that respond to platinum-based chemotherapy, thus providing a candidate predictive biomarker for this disease. Furthermore, we show that a high level of AiCNA is linked with elevated expression of a meiosis-

[§]Corresponding author: Professor Andrew Tutt, Breakthrough Breast Cancer Research Unit, 3rd Floor Bermondsey Wing, Guy's Hospital, London SE1 9RT, Tel. +44 (0)20 7188 9881, Fax: +44 (0)20 7188 3666, andrew.tutt@kcl.ac.uk.
Reprint request: Anita Grigoriadis; anita.grigoriadis@kcl.ac.uk
[*]These authors contributed equally to the work
[$]Current address: UCSF Helen Diller Family Comprehensive Cancer Center, San Francisco, California, 94158, USA.
[#]Current address: Case Western Reserve University School of Medicine, Cleveland, Ohio, 44106, USA.

Disclosure of Potential Conflicts of Interest: J. Watkins, A. Grigoriadis and A.N.J. Tutt are inventors on a pending patent application based upon this work.

associated gene *HORMAD1*. Elevated *HORMAD1* expression suppresses RAD51-dependent HR and drives the use of alternative forms of DNA repair, the generation of AiCNAs as well as sensitising cancer cells to HR targeting therapies. Our data therefore provides a mechanistic association between *HORMAD1* expression, a specific pattern of genomic instability and an association with response to platinum-based chemotherapy in TNBC.

Keywords

Breast cancer; DNA damage and repair mechanisms; New algorithms; Methodology for SNP data analysis; Modulation of DNA repair

Introduction

Women with germline mutations in either the *BRCA1* or *BRCA2*, the products of which are required for DNA double strand break repair by homologous recombination (HR) (1, 2), have an increased risk of developing breast and ovarian cancer. *BRCA1* mutations are particularly prevalent in triple-negative breast cancers (TNBCs), a subtype of breast cancer defined by a lack of elevated HER2 expression, oestrogen receptor (ER) and progesterone receptor expression, and molecularly similar high-grade serous ovarian cancers (HGSC) (3). Many TNBCs and HGSCs are characterised by high mitotic indices and highly unstable genomes, observations which have stimulated research into chromosomal instability as a biomarker of response to platinum-based chemotherapies, and also into synthetic lethal agents such as the poly (ADP-ribose)-polymerase (PARP) inhibitors (4, 5). The potential causes and consequences of chromosomal instability phenotypes are likely to be diverse, and encompass structural-level copy number aberrations (CNAs) and loss of heterozygosity (LOH) (6). The use of high-resolution single nucleotide polymorphism (SNP) arrays and associated methods of analysis are now commonly used to detect CNAs and LOH in tumours (7, 8). In the context of TNBC, several array-based CNA/LOH signatures of platinum-based drug response and *BRCA* inactivation have recently been developed (9-12). These include a telomeric allelic imbalance score (N_{tAI}) which predicts sensitivity to platinum analogues (10), a homologous repair defect (HRD) score designed to comprehensively assess the impairment of HR in addition to *BRCA1* and *BRCA2* deficiency (9), the *Large Scale Transition* measurement, a signature of *BRCA1* inactivation-associated genomic instability (11), as well as an array comparative genomic hybridisation-based classifier designed to identify germline *BRCA1/2* mutant carriers (13). Although promising, current measures do not suggest mechanisms that either compensate for underlying repair deficiencies or drive the observed genomic instability. Moreover, the observation that *BRCA1/2* inactivation is not the only driver of genomic instability in TNBC (14, 15) has prompted the search for alternative mechanisms that drive HR dysfunction and subsequent chromosomal instability.

Here, we demonstrate that scores of allelic imbalance are higher in TNBCs responding to platinum-based chemotherapy. Furthermore, we identify and functionally validate HORMAD1, a cancer testis antigen involved in the promotion of non-conservative recombination in meiosis (16-18) as a novel driver of the allelic imbalance phenotype in

TNBC. HORMAD1 mediates these effects through suppression of RAD51-dependent HR and in doing so drives 53BP1-dependent non-homologous end-joining (NHEJ). Additionally, HORMAD1 positivity correlated with a better response to HR defect-targeting agents both in TNBC cell lines and clinical trial data, and may add value to *BRCA1/2* mutation testing for platinum treatment in unselected TNBC patients.

Results

TNBCs exhibit distinct types and levels of chromosome scarring

To comprehensively capture the variety of genomic aberrations that TNBCs exhibit, we interrogated the genome-wide Affymetrix SNP6.0 array profiles of an unpublished cohort of 126 TNBCs from Guy's Hospital King's College London ("KCL TNBC"). We obtained allele-specific copy number profiles for 111 of these, and confirmed several previously identified recurrent (>25% of cases) gains, losses and regions of copy number neutral LOH (CnLOH) (12, 19) (Supplementary Fig. S1A-C). Furthermore, approximately 13% of KCL TNBCs (Supplementary Table S1) harboured chromothripsis-like features (20). In order to unravel this complexity and extract genomic patterns to provide both biological and clinical insights, we devised three categories of genomic scars that might each be generated by a distinct combination of mutational processes: (i) allelic-imbalanced CNAs (S_{AiCNA}), which potentially reflect defects arising from an increased reliance on error-prone forms of double strand break repair such as NHEJ or non-allelic HR; (ii) copy-neutral LOH (S_{CnLOH}), which might arise from regions of non-conservative allelic HR (6, 21, 22); and (iii) allelic-balanced CNAs (S_{AbCNA}), which may be indicative in large part of whole genome doubling (23) (Materials and Methods, Supplementary Fig. S2 and Supplementary Table S2). In addition, we derived a combined score, S_{Ai} (the sum of S_{AiCNA} and S_{CnLOH}) to capture impaired conservative double strand break repair irrespective of the precise biological mechanism or mechanisms that created it (10). All four scores were collectively termed "scores of chromosomal instability scarring" (SCINS).

We applied SCINS to our KCL TNBCs and observed that the total burden as well as the relative degree of S_{AbCNA}, S_{AiCNA} and S_{CnLOH} differed substantially over the cohort. While some TNBCs showed no SCINS-defined genomic alterations, many harboured numerous scars with one possessing a combined allelic imbalance score (S_{Ai}) of approximately 80 (Fig. 1A). For two TNBCs, the scarring burden was entirely attributable to S_{AiCNA}, while others showed an almost 99% contribution from S_{CnLOH}, and some exhibited a roughly equal share of S_{AiCNA} and S_{CnLOH} (Fig. 1A). These results were not influenced by normal cell contamination, since no association between tumour content and any of the SCINS was observed ($P > 0.5$, Kruskal-Wallis test). A less chromosomally biased distribution was noted for S_{AiCNA} and S_{AbCNA} (Fig. 1A heatmap and Supplementary Fig. S3A-C), whereas genomic segments contributing to S_{CnLOH} were concentrated on chromosomes 14 and 17 (Fig. 1A heatmap, Supplementary Figs. S3A-C and S4A-D).

To investigate whether S_{AiCNA}, S_{CnLOH} and S_{AbCNA} were comparable across different datasets, we obtained copy number profiles for 97 METABRIC TNBCs (24), 80 TCGA TNBCs (25), and 71 pretreated TNBCs from the gemcitabine, carboplatin and iniparib-treated neoadjuvant PrECOG 0105 (NCT#00813956) (26) study ("PrECOG TNBCs") as

well as a panel of 38 breast cell lines, 20 of which were triple-negative. We applied SCINS to these datasets and demonstrated that overall, our scores were recapitulated. Pairwise comparisons of the core SCINS measures between the four TNBC cohorts and the panel of cell lines revealed no significant difference between the distributions of S_{CnLOH} and S_{Ai} (Fig. 1B). However, whereas the distribution of S_{AiCNA} was similar among TNBCs, and likewise for S_{AbCNA} ($P > 0.15$, KS test; Fig. 1B), the distributions in ER-positive cell lines differed significantly ($P < 0.05$, KS test; Fig. 1B) reinforcing evidence for the particular similarities in genomic instability profiles between TNBC and their cell line models (27).

Correlation analyses provided validation that each scar was capable of capturing independent information with only moderate correlation observed at most. We found S_{AiCNA} to be largely independent of S_{CnLOH} across all datasets (Fig. 1C). To assess the relationship between SCINS and published measures of HR deficiency and platinum response, we also scored tumours for the previously described N_{tAi} measure of telomeric allelic imbalance (10) and an approximation of the HRD score (9), which we term S_{LOH}. As expected, our composite allelic imbalance score, S_{Ai}, most closely tracked N_{tAi} while a modest correlation was observed between S_{CnLOH} and S_{Ai}, and S_{LOH} (Fig. 1C). These results support the segregation of the constituent scores of SCINS as a means of providing different forms of information on the nature of genomic instability in such tumours.

Platinum agent sensitivity correlates with S_{AiCNA} and S_{Ai} in tumours

Platinum salts have emerged as potentially selective therapeutics for the treatment of TNBC (28). Since the repair of platinum adducts can induce single and double stranded DNA breaks that require HR for their repair and cell survival we sought to test whether our measures of genome instability correlated with any specific sensitivity to carboplatin response (Materials and Methods) in the PrECOG TNBCs and a cohort of HGSCs from TCGA where whole genome SNP profiles for which such data was available. Our composite allelic imbalance scar, S_{Ai}, proved to be significantly higher in cancers responding to platinum-based chemotherapy (Fig. 1D). We next evaluated the individual contributions made by the two constituent components of S_{Ai}, S_{AiCNA} and S_{CnLOH}. In the PrECOG TNBC study, S_{AiCNA} but not S_{CnLOH} was significantly associated with platinum-based chemotherapeutic response (Fig. 1E and F) whereas both S_{AiCNA} and S_{CnLOH} were significantly linked with an enhanced platinum-based chemotherapeutic response in HGSC (Fig. 1E and F). Stratification by *BRCA1/2* status revealed higher levels of allelic imbalance in *BRCA1/2* mutated cancers overall, supporting the concept that S_{AiCNA} is indicative of HR deficiency. Interestingly, among the wildtype *BRCA1/2* tumours in both cohorts, those patients that responded to platinum treatment had higher S_{AiCNA} and S_{Ai} (Fig. 1D and E). Taken together, our results support the potential utility of allelic imbalance-based measures as markers of response to DNA damaging chemotherapeutics but further highlight the particular contribution of S_{AiCNA} in driving much of the association with response in TNBC. Of note, the presence of a substantial number of platinum-responsive, high S_{Ai} tumours without *BRCA1/2* mutation underscores the fundamental need to identify alternative mechanisms at play that underpin this form of chromosomal instability and its association with platinum sensitivity.

SCINS-based class discovery identifies high *HORMAD1* expression associated with allelically-imbalanced tumours

Next, we sought to identify candidate drivers of the SCINS-defined clusters by interrogating the transcriptional profiles associated with each. Therefore, we conducted hierarchical clustering of the KCL, METABRIC and PrECOG TNBCs separately using S_{AiCNA}, S_{CnLOH} and S_{AbCNA} as covariates. Matching gene expression data was available for 77, 97 and 59 KCL, METABRIC and PrECOG TNBCs, respectively. In all datasets, we observed two stable top-level clusters, which divided the cohort into a major cluster of ∼60% of samples, and a minor group of TNBCs scoring low for all SCINS, referred to hereafter as 'Lo-SCINS' (green branch of Figs. 2A, B and Supplementary Fig. S5A). The major group further separated into two distinct and robust subclusters (Figs. 2A, B and Supplementary Fig. S5A). Examination of the three core SCINS across these two subclusters, revealed that in both cohorts, one cluster (blue branches, Figs. 2A, B and Supplementary Fig. S5A) comprised samples with high S_{CnLOH} (Figs. 2A, B, and Supplementary Fig. S5A, boxplots), which we termed 'Hi-CnLOH'. In contrast, the second subcluster (red branches, Figs. 2A, B and Supplementary Fig. S5A) was composed of a third of samples, and featured tumours with the highest S_{AiCNA} (Figs. 2A, B, and Supplementary Fig. S5A, boxplots), hereafter termed 'Hi-AiCNA'. In contrast, S_{AbCNA} did not significantly differ between the Hi-AiCNA and Hi-CnLOH clusters. On the basis of these stable SCINS-defined TNBC clusters, we next sought to define some of the transcriptional events associated with these different genomic instability measures. Starting with the top-level partitions, we performed SAM analysis and identified *HORMAD1*, a cancer testis antigen that is normally exclusively expressed in germline cells and known to have function in meiosis, to be the top-ranked differentially expressed gene by fold change among tumours in the Hi-AiCNA/Hi-CnLOH cluster of the KCL cohort (Fig. 2C and Supplementary Table S3). In agreement, higher expression of *HORMAD1* was also seen in the Hi-AiCNA/Hi-CnLOH cluster of the METABRIC and PrECOG TNBC cohorts (Fig. 2D, Supplementary Fig. S5B and Supplementary Table S3) despite only modest correlations between the gene expression values of the datasets (Supplementary Fig. S5C).

Having established a link between *HORMAD1* expression and our Hi-AiCNA/Hi-CnLOH group of tumours, we next set out to refine this analysis by investigating which genes were associated with distinct forms of allelic imbalance. We interrogated the transcriptional profiles of the Hi-AiCNA, Hi-CnLOH and Lo-SCINS clusters (Figs. 2E and F), compared the resultant gene lists from each cohort, and found 19, 5 and 45 genes to be common to the Lo-SCINS, Hi-AiCNA and Hi-CnLOH-specific clusters, respectively (Fig. 2G and Supplementary Table S3) with *HORMAD1* present in the common gene list of the Hi-AiCNA clusters (Fig. 2H), suggesting a specific association with S_{AiCNA} scarring. A second gene involved in meiotic recombination, *PSMC3IP*, was also present among genes associated with the high S_{AiCNA} clusters.

Investigation of the expression pattern of *HORMAD1* revealed a clear bimodality among TNBCs (Fig. 3A), allowing dichotomisation of the population with approximately 60% showing high *HORMAD1* expression in each cohort (46 of 77 for KCL, and 61 of 97 for METABRIC). Using gene expression signatures as surrogate markers of different aspects of

genomic instability and genetic lesions known to be important in TNBC (Supplementary Table S4), we found many of these signature scores to be significantly higher in the high *HORMAD1* in comparison to the low *HORMAD1* group of samples (Fig. 3B and Supplementary Fig. S6A-J). Examination of *HORMAD1* expression across all breast cancer types in the KCL (29), METABRIC (24) and TCGA (25) cohorts provided further evidence for a high *HORMAD1* subgroup specifically in basal-like breast carcinomas (Fig. 3C). In contrast, we found no significant link between *HORMAD1* expression and any of the genomic scarring measures in HGSCs ($P > 0.05$; data not shown) or any evidence of bimodality.

Our finding of significant associations between signatures of genomic instability-linked pathways, such as those involving *TP53* mutation and *Rb* loss, and high *HORMAD1* expression (Supplementary Fig. S6A-J) prompted us to conduct functional experiments to test whether HORMAD1 overexpression could cause chromosomal instability.

HORMAD1 is expressed in the nucleus of breast cancer cells in both cell lines and tumours

We turned to cellular models of breast cancer to provide a tractable system to investigate the consequences of *HORMAD1* expression and whether the relationship with S_{AiCNA} was causative. We first confirmed a relationship between *HORMAD1* expression and S_{Ai} in a panel of 23 breast cancer cell lines for which gene expression was available (Fig. 4A). The bimodal expression pattern in TNBC was replicated at the protein level in cellular models where HORMAD1 protein was expressed in 5 of the 9 ER and HER2 negative cell lines examined (HCC70, HCC1143, MDAMB436, HCC38 and CAL51) with levels showing good concordance with gene expression data (Fig. 4B). Furthermore, no expression of HORMAD1 protein was seen in two non-transformed mammary epithelial cells, MCF10A and HMEC (Fig. 4B). In meiotic cells, HORMAD1 localises to the nucleus (17) and can recognise aberrant DNA structures possibly due to its chromatin-associated HORMA domain (30). Subcellular fractionation of cells in triple-negative HCC1143 breast cancer cells confirmed the presence of HORMAD1 in the nuclear fraction (Fig. 4C), where it appears to be constitutively associated with chromatin in a DNA damage-independent manner (Fig. 4D). Moreover, immunofluorescence analysis (IF) using a HORMAD1-specific antibody showed nuclear staining of endogenous protein in HCC1143 and of protein expressed from an exogenous cDNA in SUM159. No nuclear staining was seen in the HORMAD1-negative parental SUM159 cell line (Fig. 4E). Additionally, expression of GFP tagged HORMAD1 in SUM159 also demonstrated nuclear localisation (Supplementary Fig. S7A). Induction of DNA damage by IR or HU did not induce a detectable change in HORMAD1 localisation by IF (Supplementary Fig. S7B). A similar nuclear staining pattern was also observed by immunocytochemistry in the *HORMAD1* expressing cell lines, HCC38 and HCC70 (Supplementary Fig. S8A). Interrogation of tissue microarrays confirmed nuclear localisation of HORMAD1 in primary TNBC (Supplementary Fig. S8A). To quantify HORMAD1 protein levels in primary tumours, we carried out protein extractions and western blots (Fig. 4F, Supplementary Fig. S8B). HORMAD1 protein expression was detectable in 13 of 15 tumours identified as having high *HORMAD1* by gene expression. Protein expression in these tumours was at comparable levels to that in HORMAD1-

expressing TNBC cell line models (Fig. 4F). As anticipated, tumours in the low *HORMAD1* transcript group had no detectable protein (Fig. 4F).

HORMAD1 expression drives S_{AiCNA} and chromosomal instability

In breast cancer cell lines, *HORMAD1* expression was significantly associated with S_{Ai} (r_s = 0.46, P = 0.019; Fig. 4A). Although we had established an association between *HORMAD1* expression and genomic instability in triple-negative breast tumours and cell line models, it was not at this point clear whether elevated *HORMAD1* expression drove genomic instability or was a consequence. To this end, we created stable HORMAD1 and control LacZ-expressing populations of SUM159 cells, a triple-negative cell line model with relatively low levels of genomic instability (31) and low *HORMAD1* expression. Expression of HORMAD1 or LacZ did not change the growth rate of SUM159 cells (Supplementary Fig. S9A). In order to test whether HORMAD1 expression induced the similar genome scarring patterns as those associated with elevated *HORMAD1* expression in primary TNBCs, we compared the SNP6.0 array profiles and SCINS from HORMAD1 and LacZ-expressing populations of cells grown under the same conditions for the same period of time over two independent experiments. We found both S_{AiCNA} and S_{Ai} to be higher in the *HORMAD1*-expressing SUM159-HORMAD1-V5 cells compared to the control-treated SUM159-LacZ-V5 cells, with an average fold change in these scar measures of 4 and 1.5, respectively (Fig. 5A). No increase in S_{CnLOH} was observed in SUM159-HORMAD1-V5 cells compared to SUM159-LacZ-V5 cells (Fig. 5A). This observation was consistent with the hypothesis that HORMAD1 might be capable of driving the generation of specific genomic scars, specifically, allelic imbalances accompanied by copy number change.

We also investigated whether HORMAD1 expression might drive structural chromosomal aberrations in these cells. Metaphase spreads were prepared from SUM159-HORMAD1-V5 and SUM159-LacZ-V5 populations, and chromosomal abnormalities counted (Fig. 5B). Overall, SUM159-HORMAD1-V5 cells had a 4-fold greater number of structural chromosomal abnormalities compared to SUM159-LacZ-V5 cells (P = 0.002) with a significant increase in acentric fragments and chromatid loops (P = 0.038 and P = 0.021, respectively; Fig. 5B).

Aberrant nuclear structures such as micronuclei (MN), nuclear buds (NBUD) and nucleoplasmic bridges (NPB) are biomarkers of induced genotoxic events and chromosomal instability (32). We therefore assessed SUM159-HORMAD1-V5 and SUM159-LacZ-V5 populations for the presence of these nuclear anomalies (Fig. 5C). Overall, SUM159-HORMAD1-V5 cells exhibited a 3.25-fold increase in MN, NBUD and NPB compared to SUM159-LacZ-V5 cells. Individually, fold increases of 2.2, 2.7 and 2 were observed for MN, NBUD and NPB, respectively (Fig. 5C).

HORMAD1 is involved in many aspects of meiotic recombination, in which RAD51-dependent equal sister chromatid recombination is inhibited in favour of DMC1-mediated recombination and cross over formation with the homologous chromosome (33-35). For this reason, we examined whether inappropriate HORMAD1 expression in a mitotic cell context might suppress conservative HR in TNBC cell line models. We used the DR-GFP assay to assess conservative HR of an I-SceI endonuclease-induced double strand break (36).

Overexpression of HORMAD1 in this system caused a 55% reduction in HR in SUM159 (HORMAD1-negative) cells (Fig. 5D). Overexpression of HORMAD1 in the HORMAD1 low expressing cell line, CAL51, also caused a 36 % decrease in HR activity (Fig. 5E, Supplementary Fig. S9B). In contrast, siRNA-mediated knockdown of HORMAD1 in HCC1143 and MDAMB436 (both HORMAD1-positive lines) caused an increase in HR (100% and 55% increases, respectively; Fig. 5F, Supplementary Fig. S9C). Ectopic expression of HORMAD1 in mouse ES cells with an integrated DR-GFP reporter also led to reduced HR levels (Supplementary Fig. S9D). This data suggests that HORMAD1 is capable of regulating HR activity in established breast cancer cells but also in non-transformed cells. To assess whether HORMAD1-expressing cells show failure to repair spontaneous DNA double strand breaks, we assessed the number of spontaneous γ-H2AX nuclear foci and found SUM159-HORMAD1-V5 cells to have more than twice the mean number of γ-H2AX nuclear foci, a biomarker of double strand breaks, compared to SUM159-LacZ-V5 cells (fold increases of 7.5 and 3.3, respectively; Fig. 5G, Supplementary Fig. S9E). To further test the hypothesis that HORMAD1 modulates RAD51-dependent HR and double strand break repair, we measured hydroxyurea (HU) and IR-induced RAD51 nuclear focus formation, a biomarker of HR, and observed a significant reduction in the number of DNA damage-induced RAD51 foci in SUM159-HORMAD1-V5 cells when compared to SUM159-LacZ-V5 cells (Fig. 5H, Supplementary Fig. S9F). Transient expression of HORMAD1 in this assay caused a modest reduction in SUM159 cell growth (80%, P=0.05) and a statistically significant increase (P=0.01) in the proportion of cells in S-phase (37%) compared to empty vector-transfected SUM159 (27.8%, Supplementary Fig. S10A and B). Alterations in cell cycle distribution, specifically a reduction in the number of S-phase cells, can result in an apparent reduction in HR activity. However, since transient HORMAD1 expression causes an increase in the proportion of cells in S-phase, this is unlikely to be an explanation for the reduction in HR activity that we observe (Supplementary Fig. S10B). Conversely, siRNA-mediated knockdown of HORMAD1 in MDAMB436 and HCC1143 caused a reduction in the percentage of cells in S-phase (Supplementary Fig. S10C), and is equally unlikely to explain the increase in HR activity that we observe in these cells after HORMAD1 knock down. In fact, we suggest that HORMAD1-induced impairment of the repair of replication-associated DNA damage is likely to cause an accumulation of cells in S-phase.

Having observed both an impairment of HR and an increase in specific forms of chromosomal instability in HORMAD1-overexpressing cells, we asked whether such cells exhibited increased levels of NHEJ repair, a DNA double strand break process that is commonly upregulated in response to HR deficiency. NHEJ activity was assessed by measuring the induction of 53BP1 focus formation by both IR and HU (Fig. 5I, Supplementary Fig. S11A) and the repair of I-SceI endonuclease-induced double strand breaks in the previously-validated EJ5 NHEJ GFP reporter assay (37) (Fig 5J). In both assays, SUM159-HORMAD1-V5 cells showed significantly increased levels of NHEJ activity compared with SUM159-LacZ-V5 cells (Fig. 5I-J). A similar increase in NHEJ activity was observed with transient transfection of HORMAD1 suggesting that expression of HORMAD1 had a direct, acute effect on NHEJ activity (Supplementary Fig. S11B and S11C). Furthermore, despite long term exposure to endogenous HORMAD1 expression,

knockdown of HORMAD1 in HCC1143 reduced EJ5 NHEJ GFP reporter-measured NHEJ (Fig. 5J) and damage induced 53BP1 focus formation (Supplementary Fig. S12A) with a modest non-significant increase in nuclear RAD51 foci also observed (Supplementary Fig. S12B).

HORMAD1 overexpression drives sensitivity to HR defect-targeting drugs in TNBC

Given the association between high S_{Ai}, and in particular high S_{AiCNA}, and platinum salt sensitivity (Fig. 1 and Supplementary Fig. S13A-F), along with the established observation that HR-deficient cells show increased sensitivity to platinum salts and PARP inhibitors (38), we sought to examine whether there was a causative role for HORMAD1 in increasing platinum agent sensitivity. As such, we investigated the effect of HORMAD1 overexpression on the sensitivity of SUM159 and CAL51 to cisplatin. Consistent with the effect in the DR-GFP and RAD51 HR assays, HORMAD1 overexpression increased sensitivity of both SUM159 and CAL51 cell lines to cisplatin with HORMAD1 expression decreasing cisplatin SF50 from 10.8 μM to 4.4μM in SUM159 ($P < 0.0001$), and from 7.4 μM to 3.3μM in CAL51 ($P = 0.003$) (Fig. 6A). Next, we assessed whether breast tumour cell line models with elevated *HORMAD1* expression (Fig. 4B) exhibited sensitivity to potent small molecule PARP inhibitors, which have previously been shown to selectively target tumour cells with *BRCA1* or *BRCA2* defects (39). Using dose response survival experiments in cells exposed to the clinical PARP1/2 inhibitor, olaparib (AZ/KuDOS) (39), we found that MDAMB436, HCC1143, HCC70 and CAL51 models, each of which expressed elevated levels of *HORMAD1*, all exhibited a moderate level of sensitivity. This was in contrast to the relative olaparib insensitivity observed in *HORMAD1*-deficient HS578T, BT20, MDAMB231, SKBR3 and SUM159 models (Fig. 6B and C). To test if elevated HORMAD1 expression could directly drive PARP inhibitor sensitivity, we examined the PARP inhibitor sensitivity of SUM159-HORMAD1-V5 and SUM159-LacZ-V5 populations. SUM159-HORMAD1-V5 cells showed a significantly greater sensitivity to olaparib (left, $P = 0.0001$, Fig. 6D). To eliminate the possibility that this observation might be specific to olaparib, we assessed the sensitivity of these cells to a novel, hyperpotent clinical PARP inhibitor, BMN673 (40) (right, $P = 0.0001$, Fig. 6D). The PARP inhibitor sensitization, resulting from overexpression of HORMAD1, whilst significant was relatively modest compared to that produced by *BRCA2* mutation (Fig. 6D). This is consistent with the moderate reduction in HR, sufficient to induce genomic instability without profound cell cycle arrest, seen in previously described assays (Figs. 5D, 5E, 5H) and indicates that HORMAD1 expression partially rather than completely ablates HR competency.

We looked at the reciprocal effect of HORMAD1 siRNA on the sensitivity of the high HORMAD1 cell line HCC1143 to cisplatin and the PARP inhibitor BMN673 (Supplementary Fig. S14A and S14B). Despite long term exposure to endogenous HORMAD1 expression and potential adaptation, we observed the anticipated modest but statistically significant reduction in sensitivity to BMN673 following HORMAD1 knockdown consistent with the effects observed on NHEJ, 53BP1 and RAD51 focus formation (Fig. 5J and Supplementary Fig S12). However, no effect on cisplatin sensitivity in this cell line was observed, indicating that although expression of HORMAD1 is sufficient to induce platinum agent sensitivity it is not always necessary. Many DNA repair

defects contribute to cisplatin sensitivity, and HORMAD1 knockdown in a long term HORMAD1 adapted cell line is unlikely to significantly change response to a chemotherapy drug acting through several mechanisms. In contrast, PARP inhibition has a more selective mechanism of action, more directly related to its specific targeting of HR dysfunction and potentially more sensitivity to *HORMAD1* expression levels.

Having demonstrated in cell line models that HORMAD1 is capable of driving sensitivity to HR defect-targeting drugs, we examined the applicability of HORMAD1 and the three allelic imbalance-based SCINS, when measured in pretreatment samples, to predict therapeutic response in the trial data (NCT#00813956) (26). This single arm trial treated patients with primary TNBC or *BRCA1/2* mutation-associated breast cancer with the combination of gemcitabine and carboplatin, and the investigational agent, iniparib which has no validated mechanism of action and is considered unlikely to have had any dominant effect on tumour response based on randomised trial data comparing gemcitabine and carboplatin alone with the addition of iniparib (41). PrECOG TNBCs with overlapping SNP and gene expression data were dichotomised into high (n = 29) and low (n = 30) *HORMAD1*-expressing cases based on the bimodality of gene expression, resulting in 43% and 69% responders in the HORMAD1-low and HORMAD1-high group, respectively (Fig. 6E). Receiver operating characteristic (ROC) analysis revealed *BRCA1/2* mutation status to have high specificity for treatment response but much poorer sensitivity than dichotomised *HORMAD1* expression and allelic imbalance-based SCINS (Supplementary Fig. S15). This indicates that while patients with mutations in *BRCA1/2* carry a very high probability of response, a spectrum of response is observed in those with sporadic TNBCs, many of which are *BRCA1/2* wildtype (4, 5). We therefore asked whether the performance of *BRCA1/2* mutation status in predicting platinum response could be enhanced by supplementation with *HORMAD1* expression or allelic imbalance-based SCINS. We used ROC analysis to define cutoffs that maximised the balanced accuracy of a predictor, and found that combining *HORMAD1* expression or the allelic imbalance-based SCINS with *BRCA1/2* mutation status lead to an improvement in accuracy over that for each predictor alone (Fig. 6F, yellow and blue bars). Given that *HORMAD1* might be informative of platinum response independently of *BRCA1/2* mutation, we looked within the *BRCA1/2* wildtype subpopulation of the PrECOG dataset after first confirming that there was no substantial shift in the distribution of or cutoff for *HORMAD1* bimodal expression (Supplementary Fig. S16A and S16B). We found the balanced accuracy to be either maintained (*HORMAD1*) or improved (allelic imbalance-based SCINS) within this subset of TNBCs when compared to the accuracies of the single markers in the whole population (Fig. 6F, orange bars). These findings suggest that *HORMAD1* and the allelic imbalanced-based SCINS may find utility either within a *BRCA1/2* proficient setting or in combination with *BRCA1/2* mutation testing.

Discussion

TNBCs are characterised by high levels of chromosomal instability and therapies leveraging on DNA repair defects have emerged with varying degrees of success. In this study, we have developed an approach to capture diverse genomic patterns in TNBC, which may report the activity of different combinations of mutational mechanisms. One such chromosomal aberration, S_{AiCNA}, was associated with platinum sensitivity in neo-adjuvantly treated

TNBC and HGSC, even among *BRCA1/2* proficient cases. Transcriptional profiling of TNBCs grouped on the basis of different genomic aberrations identified the mis-expression of the meiotic cancer testis antigen, *HORMAD1* as a novel driver of genome instability. Consistent with the notion of S_{AiCNA} as a measure of defective HR, *HORMAD1* expression negatively regulated HR activity in cell lines and led to generation of micronuclei and structural chromosomal aberrations. Thus, we provide the first direct experimental evidence of the causative role of a gene whose normal function is restricted to the inhibition of conservative meiotic sister chromatid HR and creation of genetic diversity, in the generation of potentially clinically relevant genomic scars of HR deficiency.

Mutational signatures and genomic scars have been shown to represent reasonable surrogates of *BRCA1/2* mutation and platinum salt sensitivity, and are currently being tested as companion diagnostics in prospective PARP inhibitor trials for HGSC (NCT#01891344) (9-12). By generating multiple scores, we expanded on these approaches to uncover the granularity of genomic alterations present in TNBC. We show that each scar, while largely independent of the others, had a consistent distribution across 4 independent TNBC cohorts. The most prevalent and informative genomic scar for platinum sensitivity was S_{AiCNA}, pointing to the frequent activation of error-prone DNA repair processes in these tumours.

Taking account of the meiotic function of HORMAD1 in promoting HR with non-sister chromatid templates, we sought evidence of upregulation of non-conservative HR in SNP microarray data by using the number of AiCNAs associated with copy number loss between low copy number repeats as a surrogate measure of intrachromosomal non-allelic HR. Given the limitations of SNP arrays to report products of the varied forms of non-conservative homology directed repair accurately, the results are inconclusive (data not shown). Therefore, we cannot currently exclude the possibility that HORMAD1, through favouring the use of non-sister chromatid homology templates, also increases the use of non-conservative recombination between non-allelic homologous templates (33) as an additional driver of AiCNAs across the genome (Fig. 7). The absence of an increase in CnLOH associated with expression of HORMAD1 cDNA in our SUM159 model (Fig. 5A) suggests that *HORMAD1* expression in this specific context does not increase allelic forms of interhomolog recombination. However, further study in a wider range of cellular contexts is warranted.

Studies in mice have identified four major meiotic functions for HORMAD1 (18, 42, 43) (Fig. 7A). However, our understanding of its activity in mitotic cells is currently limited (44). During meiosis, cells undergo a wave of double strand break induction catalysed by the topoisomerase, SPO11, leaving stretches of single-stranded DNA to which RAD51 or DMC1 associate. DMC1 is a meiosis-specific recombinase that promotes homology-directed repair between homologous chromosomes. These events and their associated crossovers are vital for both the creation of genetic diversity but also to generate chiasmata between homologous chromosomes, which ensure accurate meiotic chromosome segregation (18, 33). HORMAD1 supports the activity of both SPO11 and DMC1. While higher expression of SPO11 and DMC1 has previously been reported in melanoma and lymphoma, respectively (45), we found no evidence for their expression in TNBC (data not shown). In meiosis, in contrast to somatic cells, most double strand breaks are repaired via homology-

directed repair using the homologous chromosome rather than the sister chromatid template with the aim of creating genetic diversity (22). HORMAD1 and its orthologs, *Hop1* and *Asy1*, support this interhomolog bias as part of the barrier to sister chromatid repair, by inhibiting RAD51 engagement with sister chromatids (Fig. 7B) (35, 43, 46). Our observations of reduced HR and RAD51 foci formation in breast cell lines point to an out-of-context activation of the barrier to sister chromatid repair occurring upon HORMAD1 expression in mitotic cells. In meiosis, this process has been shown to involve the inhibition of RAD54 (35, 46), which in mouse embryonic stem cells, is essential for RAD51 focus formation after DNA damage (47). Low levels of many RAD54 paralogs in TNBC might suggest that HORMAD1 inhibits HR and RAD51 loading via a similar mechanism. While its causative relationship with genomic instability and S_{AiCNA} suggests further study to fully define its mechanism (Fig. 7B), the abnormal expression of this germ cell protein supports the hypothesis of 'meiomitosis', low level expression of meiotic components in mitotic cells that leads to genomic instability in cancer (48). Along with *HORMAD1*, our analysis identified higher transcript levels of other meiotic genes, such as *PSMC3IP* in TNBC in high S_{AiCNA} tumours. Overexpression of truncating mutants of *PSMC3IP* involved in recombination was previously found to inhibit RAD51 focus formation in cell lines (49). In addition, *SYCP2L*, engaged in the synaptonemal complex, was of higher abundance in genomically unstable HGSCs. Thus, our data adds to evidence suggesting a potentially wider role for abnormal expression of meiotic genes in the causation of genomic instability in tumours.

In this work, we have shown that the study of the whole genome allelic landscape in TNBCs reveals significant heterogeneity between tumours in the genome instability mechanisms that correlate with sensitivity to platinum salts and PARP inhibitors that are currently being considered for unselected patients with TNBC. In contrast to previous studies identifying genomic scars of HR defects, we have both identified and functionally validated a novel driver of impaired RAD51-dependent HR, and upregulated NHEJ associated with AiCNA-related genome instability and HR defect-targeting drug sensitivity. The degree of impairment of HR and consequent sensitisation to platinum salts and PARP inhibitors, caused by inappropriate *HORMAD1* expression, is more modest than that induced by loss of function *BRCA2*, the key regulator of RAD51 in mitotic cells. However, HORMAD1 induced upregulation of non-conservative DNA repair, coupled with lack of significant impairment of cell proliferation, appears sufficient to cause acquisition of increased genomic instability in affected cell populations suggesting a significant role in mutagenesis and the aetiology of basal-like TNBC.

The bimodal expression of *HORMAD1* in TNBC, along with its restricted expression in normal tissue, suggests that further examination of this gene as a biomarker component in trials of therapies that target HR deficiency in this tumour subtype is feasible and warranted. Although further evidence from multiple independent datasets and randomised therapy trials is required, our initial findings in the PrECOG0105 trial suggest that an AiCNA measure, *HORMAD1* expression and *BRCA1/2* mutation status, as a composite predictive biomarker for platinum sensitivity may have value in patients with TNBC.

Materials and Methods

Clinical sample data

A discovery dataset comprising 142 fresh-frozen, macro-dissected primary invasive TNBCs were obtained from King's Health Partners Cancer Biobank, London, UK (referred to as KCL data). A detailed description of clinico-pathological features has been published previously (50) and is provided in Supplementary Table S1. From these, we were able to extract DNA, generate SNP6.0 data (Affymetrix, Santa Clara, CA, USA) and reconstruct copy number profiles for 111 samples. Raw data from the gene expression microarray and SNP6.0 array experiments are available for download at under the accession numbers GSE40267 and E-MTAB-2626, respectively. Further details on the samples and processing of the METABRIC, TCGA TNBC, TCGA HGSC and PrECOG TNBC cohorts are provided in the Supplementary Methods.

Cell lines and cell line data

Public SNP6.0 microarray data for cell lines was obtained from the Sanger Cell Lines Project, while for a further 18 breast cell lines, DNA was isolated and SNP6.0 copy number profiles obtained via Atlas Biolabs GmbH (Berlin, Germany). All cell lines were cultured according to the supplier's recommendations, and characterised and authenticated by short tandem repeat profiling (27). Gene expression profiling and processing for cell lines has been described previously (27). The *BRCA1/2* mutation, ER, PR and HER2 statuses of cell lines are listed in Supplementary Table S1. Cell lines were authenticated by STR profiling and only used up to 30 passages from authentication.

DNA copy number analysis

For the PrECOG and TCGA (TNBC and HGSC) datasets, matched blood samples were used as reference, while for the KCL, METABRIC and cell line data, HapMap270 samples provided by Affymetrix (Affymetrix, Santa Clara, CA, USA) were taken as the reference genome. For SNP microarray data from the polyclonal SUM159 samples transfected with either HORMAD1 or LacZ, data from the SUM159 ancestor was used as reference. For the KCL, METABRIC, PrECOG, TCGA TNBC and cell line data, allele-specific copy number profiling was performed with Tumor Aberration Prediction Suite (7), while for the TCGA HGSC dataset, allelic copy number construction was implemented using Allele-Specific Copy number Analysis of Tumors (ASCAT) (8). Further details are described in the Supplementary Methods.

Scores of chromosomal instability scarring

Segments of allele-specific copy number profiles were categorised into one of three non-overlapping types: AiCNAs, AbCNAs and CnLOH, forming the basis for SCINS (Supplementary Table S2). In brief, AiCNA was determined by calculating the proportion of the genome consisting of allelic imbalanced segments, save those segments that encompassed a whole chromosome. Next, the number of AiCNA segments greater than or equal to 8 Mbp in length but less than the length of a whole chromosome was counted and this number multiplied by the proportion (excluding whole chromosome segments) to give

the AiCNA measure (S_{AiCNA}). For CnLOH, the proportion of the genome consisting of CnLOH segments was calculated only if the segment was greater than or equal to 4 Mbp in length but less than the length of a whole chromosome. Similarly to S_{AiCNA}, the measure of CnLOH segments (S_{CnLOH}) was calculated by multiplying the proportion obtained by the number of segments. For S_{AbCNA}, the measure of AbCNA segments, the number of AbCNA segments greater than or equal to 8 Mbp in length was counted. In addition, one summary measurement was established, S_{Ai}, by summing S_{AiCNA} and S_{CnLOH} thereby capturing all allelic imbalance events. A document describing SCINS is provided as Supplementary Material. N_{tAI} was calculated using code obtained from (10) while a version of the Myriad HRD score, which we term S_{LOH}, was based upon details in (9).

Kolmogorov-Smirnov tests were used to investigate differences in the distribution of (i) the distance between adjacent aberration breakpoints, and (ii) SCINS among different cohorts. Wilcoxon rank-sum tests were employed to assess the association between SCINS and chemotherapy responders/non-responders. Fisher's exact test was used to test for independence between groups. The relationships among genomic scarring scores, and also between these scores and gene expression were measured by Spearman's rank correlation. The robustness of hierarchical clustering with Ward's criterion was evaluated using the pvclust R package (51). To test the ability of *HORMAD1* expression to predict platinum-based chemotherapeutic response in PrECOG TNBCs, logistic regression analysis was performed. Optimally accurate cutoffs were established through ROC analyses and the balanced accuracy calculated as (sensitivity + specificity)/2. All p-values are two-sided, and those with values less than 0.05 were considered significant unless otherwise stated. All microarray and statistical analyses were performed in the R statistical language environment 2.14.1 (52) using several Bioconductor packages.

Gene expression analysis

Significance Analysis of Microarrays (SAM) was used to assess differential gene expression between SCINS-defined clusters using the Benjamini-Hochberg method to correct for multiple testing. Details on the meta-analysis, gene signature analysis and grouping of tumours by *HORMAD1* expression are provided in Supplementary Methods.

Expression Vectors

The HORMAD1 (NM_032132) expression vector, pEZ-M67 (GeneCopoeia), HORMAD1 lentiviral expression vector was produced by introducing the HORMAD1 coding sequence from pEZ-M67 into the pLenti6/V5-DEST Gateway™ vector (Life technologies). The pLenti6.2/V5-GW/LacZ vector (Life technologies) was used as a negative control for the effect of lentiviral infection and selection on cells. The HORMAD1 cDNA from pEZ-M67 was additionally cloned into the pCAGGS vector for use in mouse ES cell experiments.

Small interfering RNA (siRNA)-mediated silencing

Human Silencer® Select siRNAs included a non-targeting negative control siRNA (ID: 4390843) and HORMAD1 targeting (s38456) (Ambion, Life Technologies).

Antibodies

Primary antibodies used were HORMAD1 (HPA037850, Sigma Aldrich), ß-Actin (A5316, Sigma Aldrich), Histone-H3 (9715, Cell signalling technology) CENP-A (2186, Cell signalling technology), γ-H2AX (Ab22551, Abcam), RAD51 (sc-8349, Santa Cruz Biotechnology), GAPDH (D16H11, Cell signalling technology), 53BP1 (Clone BP13, Millipore). Secondary antibodies used were Alexa Fluor 488 Goat Anti-Mouse IgG, Alexa Fluor 555 Donkey Anti-Rabbit IgG (Life Technologies) or Anti-mouse/rabbit HRP conjugate (GE).

Protein fractionation

Cells were lysed in fractionation buffer (250 mM Sucrose, 20mM HEPES (7.4), 10 mM KCl, 1.5 mM $MgCl_2$, 1 mM EDTA, 1 mM EGTA, 1mM DTT and protease inhibitors) to produce cytoplasmic fraction. Whole nuclear fractions were produced using fractionation buffer supplemented with 10% glycerol and 0.1% SDS. Nuclear soluble and insoluble fractions were produced by resuspending the nuclear pellet in (20 mM Hepes, pH 8.0, 1.5 mM, MgCl2, 25% glycerol, 420 mM NaCl, 0.2 mM EDTA, 1 mM DTT, 0.5 mM PMSF) and separated by centrifugation.

Preparation of protein lysates from primary tumours

Tumour protein lysates were prepared from paraffin embeded tumour material using Laemmli buffer. The volume of buffer used for each sample was varied dependent on cellularity and tumour surface area.

Metaphase spreads

Mitotic index was increased by treatment with colcemid and cell pellets were re-suspended in 0.075M KCL and fixed in ice-cold alcohol fixative (3:1 methanol and acetic acid). Spreads were dropped at 25°C and 50% humidity, air-dried and stained with Leishman's stain (in 1:5 buffer solution at pH 6.8). Metaphase spreads and aberrations were validated independently by a cytogeneticist.

DR-GFP homologous recombination assay

Cells were seeded into 6 well plates and transfected with 3μg of the I-SceI expression plasmid (pCBASce) and 2μg of the DR-GFP reporter using FuGENE 6 transfection reagent (Promega), GFP fluorescence was assessed by FACS 72 hours post transfection. For *HORMAD1* overexpression assays, 5μg of HORMAD1 plasmid was transfected into cells using FuGENE 6 (Promega), 24 hours prior to I-SceI/DR-GFP transfection. For knockdown assays, cells were transfected with siRNA 24 hours prior to I-SceI/DR-GFP transfection. DR-GFP assays in mouse ES cells were carried out as previously described (36).

EJ5 NHEJ assays

Transient transfection of the EJ5 NHEJ vector was used as a crude measure of total NHEJ (37). Cells were seeded and transfected with the EJ5 NHEJ and I-SceI plasmid and assessed for GFP fluorescence 72 hours later by FACS.

Immunofluorescence and micronuclei assay

Cells were fixed in 4% paraformaldehyde (Sigma-Aldrich) and permeabilised in 0.5% Triton X-100 (Sigma-Aldrich). For micronuclei assessment, cells were stained with 0.2mg/mL Hoechst (Promega). Nuclei in 25 random fields (>500 cells) were assessed for the presence of aberrant nuclear structures. For IF, cells were blocked in 20% BSA in 0.1% Triton/PBS prior to incubation with antibody. Cells were counterstained with 0.2mg/mL Hoechst. To assess foci formation random fields were taken with a fluorescent microscope and the number of foci assessed by counting >50 cells.

Cisplatin sensitivity assays

Cells were seeded into 96 and transfected with *HORMAD1* or empty expression vector using FuGENE 6 (Promega). Cisplatin was added the following day and cell viability assessed 5 days later using CellTiter-Blue (Promega). Readings were normalised to vehicle treated to give percentage survival.

PARP inhibitor sensitivity assays

Olaparib was purchased from SelleckChem. BMN673 (40) was the kind gift of Dr Len Post and Dr Jerry Shen, Biomarin Inc. PARP inhibitor dose response survival experiments were carried out in a six well plate format, using a 10-14 day exposure to PARP inhibitor as previously described (39).

Supplementary Material

Refer to Web version on PubMed Central for supplementary material.

Acknowledgments

The authors thank Profs Lars Holmberg, Henrik Moeller, and Dr Hans Garmo for statistical advice, and Ian Kesterton (Viapath/Cytogenetics) for help with cytogenetics analysis.

Financial Support: Breakthrough Breast Cancer Research funded Johnathan Watkins, Daniel Weekes, Vandna Shah, Patrycja Gazinska, Shalaka Joshi, Bhavna Sidhu, Hasan Mirza, Sarah Pinder, Anita Grigoriadis and Andrew N.J. Tutt at King's College London and Jessica Frankum, Christopher J. Lord, Alan Ashworth and Andrew N.J. Tutt at The Institute of Cancer Research. In addition, the Breakthrough Breast Cancer Research Unit at King's College London obtained funding from the National Institute for Health Research Biomedical Research Centre based at Guy's and St Thomas' NHS Foundation Trust and King's College London. Cheryl Gillett was supported by the Experimental Cancer Medicine Centre at King's College London and the Department of Health via the National Institute for Health Research comprehensive Biomedical Research Centre award. Maggie C.U. Cheang received funds from Cancer Research UK. Markus Mayrhofer and Anders Isaksson were supported from the Swedish Cancer Society. Fabio Vanoli and Maria Jasin were supported by NIH grant R01CA185660. Shaveta Vinayak, James M. Ford, Melinda L. Telli received funds from Breast Cancer Research Foundation (for correlative studies for PrECOG 0105) and the Stanford Cancer Institute (for array data generation on PrECOG 0105 samples).

References

1. Moynahan ME, Chiu JW, Koller BH, Jasin M. Brca1 controls homology-directed DNA repair. Molecular cell. 1999; 4:511–8. [PubMed: 10549283]
2. Tutt A, Bertwistle D, Valentine J, Gabriel A, Swift S, Ross G, et al. Mutation in Brca2 stimulates error-prone homology-directed repair of DNA double-strand breaks occurring between repeated sequences. The EMBO journal. 2001; 20:4704–16. [PubMed: 11532935]

3. Foulkes WD, Stefansson IM, Chappuis PO, Begin LR, Goffin JR, Wong N, et al. Germline BRCA1 mutations and a basal epithelial phenotype in breast cancer. Journal of the National Cancer Institute. 2003; 95:1482–5. [PubMed: 14519755]

4. Fong PC, Boss DS, Yap TA, Tutt A, Wu P, Mergui-Roelvink M, et al. Inhibition of poly(ADP-ribose) polymerase in tumors from BRCA mutation carriers. The New England journal of medicine. 2009; 361:123–34. [PubMed: 19553641]

5. Silver DP, Richardson AL, Eklund AC, Wang ZC, Szallasi Z, Li Q, et al. Efficacy of neoadjuvant Cisplatin in triple-negative breast cancer. Journal of clinical oncology : official journal of the American Society of Clinical Oncology. 2010; 28:1145–53. [PubMed: 20100965]

6. Tuna M, Knuutila S, Mills GB. Uniparental disomy in cancer. Trends in molecular medicine. 2009; 15:120–8. [PubMed: 19246245]

7. Rasmussen M, Sundstrom M, Goransson Kultima H, Botling J, Micke P, Birgisson H, et al. Allele-specific copy number analysis of tumor samples with aneuploidy and tumor heterogeneity. Genome biology. 2011; 12:R108. [PubMed: 22023820]

8. Van Loo P, Nordgard SH, Lingjaerde OC, Russnes HG, Rye IH, Sun W, et al. Allele-specific copy number analysis of tumors. Proceedings of the National Academy of Sciences of the United States of America. 2010; 107:16910–5. [PubMed: 20837533]

9. Abkevich V, Timms KM, Hennessy BT, Potter J, Carey MS, Meyer LA, et al. Patterns of genomic loss of heterozygosity predict homologous recombination repair defects in epithelial ovarian cancer. British journal of cancer. 2012; 107:1776–82. [PubMed: 23047548]

10. Birkbak NJ, Wang ZC, Kim JY, Eklund AC, Li Q, Tian R, et al. Telomeric allelic imbalance indicates defective DNA repair and sensitivity to DNA-damaging agents. Cancer discovery. 2012; 2:366–75. [PubMed: 22576213]

11. Popova T, Manie E, Rieunier G, Caux-Moncoutier V, Tirapo C, Dubois T, et al. Ploidy and large-scale genomic instability consistently identify basal-like breast carcinomas with BRCA1/2 inactivation. Cancer research. 2012; 72:5454–62. [PubMed: 22933060]

12. Wang ZC, Birkbak NJ, Culhane AC, Drapkin R, Fatima A, Tian R, et al. Profiles of genomic instability in high-grade serous ovarian cancer predict treatment outcome. Clinical cancer research : an official journal of the American Association for Cancer Research. 2012; 18:5806–15. [PubMed: 22912389]

13. Vollebergh MA, Lips EH, Nederlof PM, Wessels LF, Schmidt MK, van Beers EH, et al. An aCGH classifier derived from BRCA1-mutated breast cancer and benefit of high-dose platinum-based chemotherapy in HER2-negative breast cancer patients. Annals of oncology : official journal of the European Society for Medical Oncology / ESMO. 2011; 22:1561–70. [PubMed: 21135055]

14. Dann RB, DeLoia JA, Timms KM, Zorn KK, Potter J, Flake DD 2nd, et al. BRCA1/2 mutations and expression: response to platinum chemotherapy in patients with advanced stage epithelial ovarian cancer. Gynecologic oncology. 2012; 125:677–82. [PubMed: 22406760]

15. Jaspers JE, Kersbergen A, Boon U, Sol W, van Deemter L, Zander SA, et al. Loss of 53BP1 causes PARP inhibitor resistance in Brca1-mutated mouse mammary tumors. Cancer discovery. 2013; 3:68–81. [PubMed: 23103855]

16. Wojtasz L, Daniel K, Roig I, Bolcun-Filas E, Xu H, Boonsanay V, et al. Mouse HORMAD1 and HORMAD2, two conserved meiotic chromosomal proteins, are depleted from synapsed chromosome axes with the help of TRIP13 AAA-ATPase. PLoS genetics. 2009; 5:e1000702. [PubMed: 19851446]

17. Fukuda T, Daniel K, Wojtasz L, Toth A, Hoog C. A novel mammalian HORMA domain-containing protein, HORMAD1, preferentially associates with unsynapsed meiotic chromosomes. Experimental cell research. 2010; 316:158–71. [PubMed: 19686734]

18. Daniel K, Lange J, Hached K, Fu J, Anastassiadis K, Roig I, et al. Meiotic homologue alignment and its quality surveillance are controlled by mouse HORMAD1. Nature cell biology. 2011; 13:599–610.

19. Ha G, Roth A, Lai D, Bashashati A, Ding J, Goya R, et al. Integrative analysis of genome-wide loss of heterozygosity and monoallelic expression at nucleotide resolution reveals disrupted pathways in triple-negative breast cancer. Genome research. 2012; 22:1995–2007. [PubMed: 22637570]

20. Stephens PJ, Greenman CD, Fu B, Yang F, Bignell GR, Mudie LJ, et al. Massive genomic rearrangement acquired in a single catastrophic event during cancer development. Cell. 2011; 144:27–40. [PubMed: 21215367]
21. Richardson AL, Wang ZC, De Nicolo A, Lu X, Brown M, Miron A, et al. X chromosomal abnormalities in basal-like human breast cancer. Cancer cell. 2006; 9:121–32. [PubMed: 16473279]
22. Stark JM, Jasin M. Extensive loss of heterozygosity is suppressed during homologous repair of chromosomal breaks. Molecular and cellular biology. 2003; 23:733–43. [PubMed: 12509470]
23. Carter SL, Cibulskis K, Helman E, McKenna A, Shen H, Zack T, et al. Absolute quantification of somatic DNA alterations in human cancer. Nature biotechnology. 2012; 30:413–21.
24. Curtis C, Shah SP, Chin SF, Turashvili G, Rueda OM, Dunning MJ, et al. The genomic and transcriptomic architecture of 2,000 breast tumours reveals novel subgroups. Nature. 2012; 486:346–52. [PubMed: 22522925]
25. Cancer Genome Atlas N. Comprehensive molecular portraits of human breast tumours. Nature. 2012; 490:61–70. [PubMed: 23000897]
26. Telli ML, Jensen KC, Kurian AW. PrECOG 0105: final efficacy results from a phase II study of gemcitabine (G) and carboplatin (C) plus iniparib (BSI-201) as neoadjuvant therapy for triple-negative (TN) and BRCA1/2 mutation-associated breast cancer. J Clin Oncol. 2013; 31 suppl; abstr 1003.
27. Grigoriadis A, Mackay A, Noel E, Wu PJ, Natrajan R, Frankum J, et al. Molecular characterisation of cell line models for triple-negative breast cancers. BMC Genomics. 2012; 13:619. [PubMed: 23151021]
28. Liu M, Mo QG, Wei CY, Qin QH, Huang Z, He J. Platinum-based chemotherapy in triple-negative breast cancer: A meta-analysis. Oncology letters. 2013; 5:983–91. [PubMed: 23426861]
29. de Rinaldis E, Gazinska P, Mera A, Modrusan Z, Fedorowicz GM, Burford B, et al. Integrated genomic analysis of triple-negative breast cancers reveals novel microRNAs associated with clinical and molecular phenotypes and sheds light on the pathways they control. BMC Genomics. 2013; 14:643. [PubMed: 24059244]
30. Aravind L, Koonin EV. The HORMA domain: a common structural denominator in mitotic checkpoints, chromosome synapsis and DNA repair. Trends in biochemical sciences. 1998; 23:284–6. [PubMed: 9757827]
31. Forozan F, Veldman R, Ammerman CA, Parsa NZ, Kallioniemi A, Kallioniemi OP, et al. Molecular cytogenetic analysis of 11 new breast cancer cell lines. British journal of cancer. 1999; 81:1328–34. [PubMed: 10604729]
32. Fenech M, Kirsch-Volders M, Natarajan AT, Surralles J, Crott JW, Parry J, et al. Molecular mechanisms of micronucleus, nucleoplasmic bridge and nuclear bud formation in mammalian and human cells. Mutagenesis. 2011; 26:125–32. [PubMed: 21164193]
33. Liu Y, Gaines WA, Callender T, Busygina V, Oke A, Sung P, et al. Down-regulation of Rad51 activity during meiosis in yeast prevents competition with Dmc1 for repair of double-strand breaks. PLoS genetics. 2014; 10:e1004005. [PubMed: 24465215]
34. Li XC, Bolcun-Filas E, Schimenti JC. Genetic evidence that synaptonemal complex axial elements govern recombination pathway choice in mice. Genetics. 2011; 189:71–82. [PubMed: 21750255]
35. Niu H, Wan L, Baumgartner B, Schaefer D, Loidl J, Hollingsworth NM. Partner choice during meiosis is regulated by Hop1-promoted dimerization of Mek1. Molecular biology of the cell. 2005; 16:5804–18. [PubMed: 16221890]
36. Pierce AJ, Johnson RD, Thompson LH, Jasin M. XRCC3 promotes homology-directed repair of DNA damage in mammalian cells. Genes & development. 1999; 13:2633–8. [PubMed: 10541549]
37. Gunn A, Stark JM. I-SceI-based assays to examine distinct repair outcomes of mammalian chromosomal double strand breaks. Methods in molecular biology. 2012; 920:379–91. [PubMed: 22941618]
38. Rottenberg S, Jaspers JE, Kersbergen A, van der Burg E, Nygren AO, Zander SA, et al. High sensitivity of BRCA1-deficient mammary tumors to the PARP inhibitor AZD2281 alone and in combination with platinum drugs. Proceedings of the National Academy of Sciences of the United States of America. 2008; 105:17079–84. [PubMed: 18971340]

39. Farmer H, McCabe N, Lord CJ, Tutt AN, Johnson DA, Richardson TB, et al. Targeting the DNA repair defect in BRCA mutant cells as a therapeutic strategy. Nature. 2005; 434:917–21. [PubMed: 15829967]
40. Shen Y, Rehman FL, Feng Y, Boshuizen J, Bajrami I, Elliott R, et al. BMN 673, a novel and highly potent PARP1/2 inhibitor for the treatment of human cancers with DNA repair deficiency. Clinical cancer research : an official journal of the American Association for Cancer Research. 2013; 19:5003–15. [PubMed: 23881923]
41. O'Shaughnessy J, Schwartzberg L, Danso MA, Miller KD, Rugo HS, Neubauer M, et al. Phase III study of iniparib plus gemcitabine and carboplatin versus gemcitabine and carboplatin in patients with metastatic triple-negative breast cancer. Journal of clinical oncology : official journal of the American Society of Clinical Oncology. 2014; 32:3840–7. [PubMed: 25349301]
42. Kogo H, Tsutsumi M, Ohye T, Inagaki H, Abe T, Kurahashi H. HORMAD1-dependent checkpoint/surveillance mechanism eliminates asynaptic oocytes. Genes to cells : devoted to molecular & cellular mechanisms. 2012; 17:439–54. [PubMed: 22530760]
43. Shin YH, McGuire MM, Rajkovic A. Mouse HORMAD1 is a meiosis i checkpoint protein that modulates DNA double- strand break repair during female meiosis. Biology of reproduction. 2013; 89:29. [PubMed: 23759310]
44. Shahzad MM, Shin YH, Matsuo K, Lu C, Nishimura M, Shen DY, et al. Biological significance of HORMA domain containing protein 1 (HORMAD1) in epithelial ovarian carcinoma. Cancer letters. 2013; 330:123–9. [PubMed: 22776561]
45. Lindsey SF, Byrnes DM, Eller MS, Rosa AM, Dabas N, Escandon J, et al. Potential role of meiosis proteins in melanoma chromosomal instability. Journal of skin cancer. 2013; 2013:190109. [PubMed: 23840955]
46. Niu H, Wan L, Busygina V, Kwon Y, Allen JA, Li X, et al. Regulation of meiotic recombination via Mek1-mediated Rad54 phosphorylation. Molecular cell. 2009; 36:393–404. [PubMed: 19917248]
47. Tan TL, Essers J, Citterio E, Swagemakers SM, de Wit J, Benson FE, et al. Mouse Rad54 affects DNA conformation and DNA-damage-induced Rad51 foci formation. Current biology : CB. 1999; 9:325–8. [PubMed: 10209103]
48. Grichnik JM. Genomic instability and tumor stem cells. The Journal of investigative dermatology. 2006; 126:1214–6. [PubMed: 16702970]
49. Peng M, Bakker JL, Dicioccio RA, Gille JJ, Zhao H, Odunsi K, et al. Inactivating Mutations in GT198 in Familial and Early-Onset Breast and Ovarian Cancers. Genes & cancer. 2013; 4:15–25. [PubMed: 23946868]
50. Gazinska P, Grigoriadis A, Brown JP, Millis RR, Mera A, Gillett CE, et al. Comparison of basal-like triple-negative breast cancer defined by morphology, immunohistochemistry and transcriptional profiles. Modern pathology : an official journal of the United States and Canadian Academy of Pathology, Inc. 2013; 26:955–66.
51. Suzuki R, Shimodaira H. Pvclust: an R package for assessing the uncertainty in hierarchical clustering. Bioinformatics. 2006; 22:1540–2. [PubMed: 16595560]
52. 2011 RDCT. Available from: http://www.r-project.org/
53. Habermann JK, Doering J, Hautaniemi S, Roblick UJ, Bundgen NK, Nicorici D, et al. The gene expression signature of genomic instability in breast cancer is an independent predictor of clinical outcome. International journal of cancer Journal international du cancer. 2009; 124:1552–64. [PubMed: 19101988]

Abbreviation list

TNBCs	Triple-negative breast cancers
HR	homologous recombination
AiCNA	Allelic-imbalanced Copy Number Aberrations

ER	oestrogen receptor
HGSC	high-grade serous ovarian cancers
PARP	poly (ADP-ribose)-polymerase
CNAs	copy number aberrations
LOH	loss of heterozygosity
SNP	single nucleotide polymorphism
HRD	a homologous repair defect
NHEJ	non-homologous end-joining
CnLOH	copy number neutral LOH
SCINS	scores of chromosomal instability scarring
IF	immunofluorescence analysis
MN	as micronuclei
NBUD	nuclear buds
NPB	nucleoplasmic bridges
HU	hydroxyurea
ROC	Receiver operating characteristic
ASCAT	Allele-Specific Copy number Analysis of Tumors
HU	Hydroxyurea
SEM	standard error of the mean
wt	wild type
mt	mutant

Significance

Previous studies have shown correlation between mutational “scars” and sensitivity to platinums extending beyond associations with *BRCA1/2* mutation, but do not elucidate mechanism. Here a novel allele-specific copy number characterisation of genome instability identifies and functionally validates the inappropriate expression of the meiotic gene *HORMAD1* as a driver of HR deficiency in TNBC, acting to induce allelic imbalance and moderate platinum and PARP inhibitor sensitivity with implications for the use of such “scars” and expression of meiotic genes as predictive biomarkers.

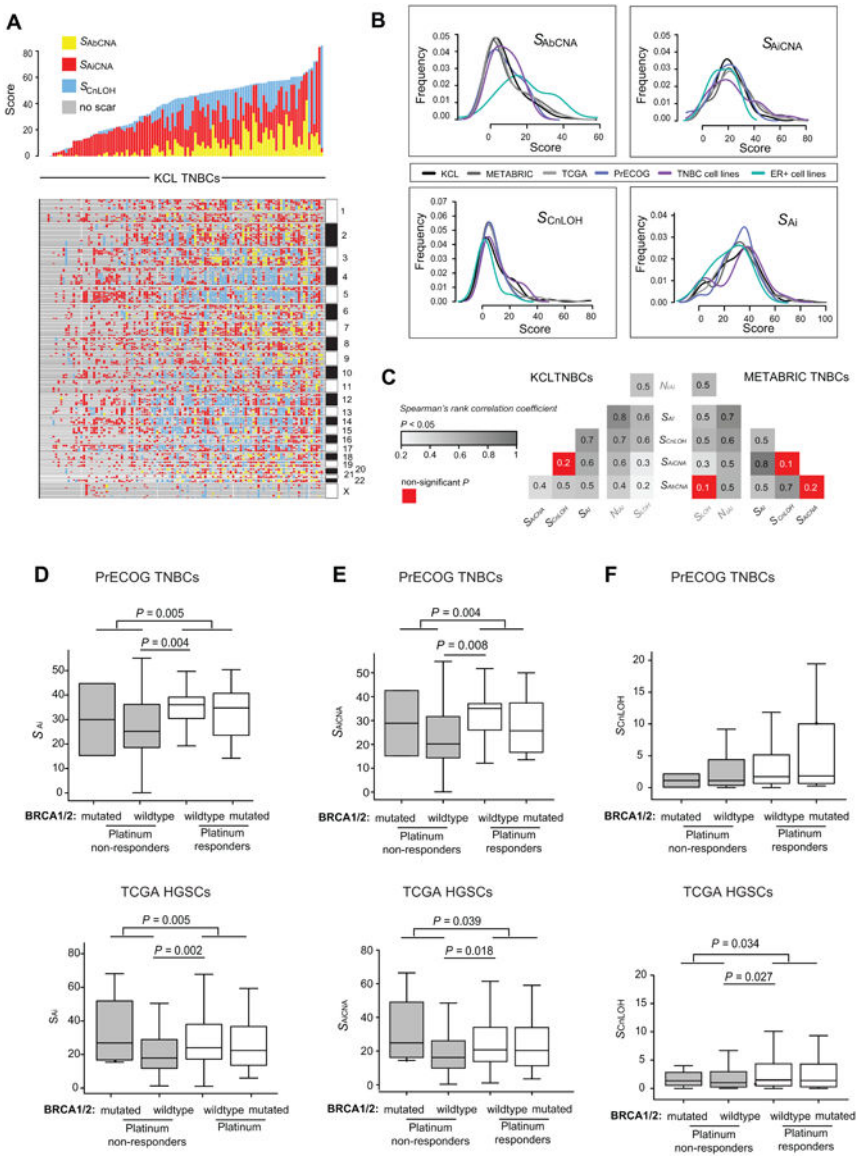

Figure 1. The extent and nature of allelic imbalance genomic scarring differentially associate with platinum-based chemotherapy sensitivity in TNBC and HGSC

A, bar plot showing the contributions for each sample in the KCL dataset (111 TNBCs) of S_{AbCNA} (yellow), S_{AiCNA} (red) and S_{CnLOH} (blue). Samples are displayed from left to right in ascending order of total genomic scarring burden. Each column in the heatmap underneath corresponds to a sample in the bar plot, and depicts the genomic location of each type of scar. Chromosome number on the vertical axis runs from 1 at the top to × at the bottom. **B,** density plots illustrating the distribution of the three core SCINS and S_{Ai} across the KCL dataset (black curve), the METABRIC dataset (dark grey curve), TCGA TNBC dataset (grey curve), PrECOG TNBC dataset (blue curve), the TNBC cell line panel (purple curve) and the ER-positive breast cancer cell lines (turquoise curve). Using a Kolmogorov-Smirnov test, p-values were evaluated for each distribution of SCINS between each combination of dataset pairs. All comparisons bar that between ER-positive cell lines and the rest had $P > 0.05$. **C**, correlation between the SCINS (black font), S_{LOH} and N_{tAI}

measures (grey font) of genomic scarring in KCL TNBCs (right panel) and METABRIC TNBCs (left panel). The strength of correlation is measured by Spearman's rank correlation coefficient and ranges from high (black) to low (white). Correlations for which $P > 0.05$ are coloured red. **D, E** and **F**, box plots depicting the distribution of S_{Ai} (**D**), S_{AiCNA} (**E**), and S_{CnLOH} (**F**) in PrECOG TNBCs (top panel plots) and TCGA HGSCs (bottom panel plots), stratified by platinum-based chemotherapeutic responder status, and sub-stratified by *BRCA1/2* mutation status. P-values were obtained using a Wilcoxon rank-sum test. Only significant p-values are shown.

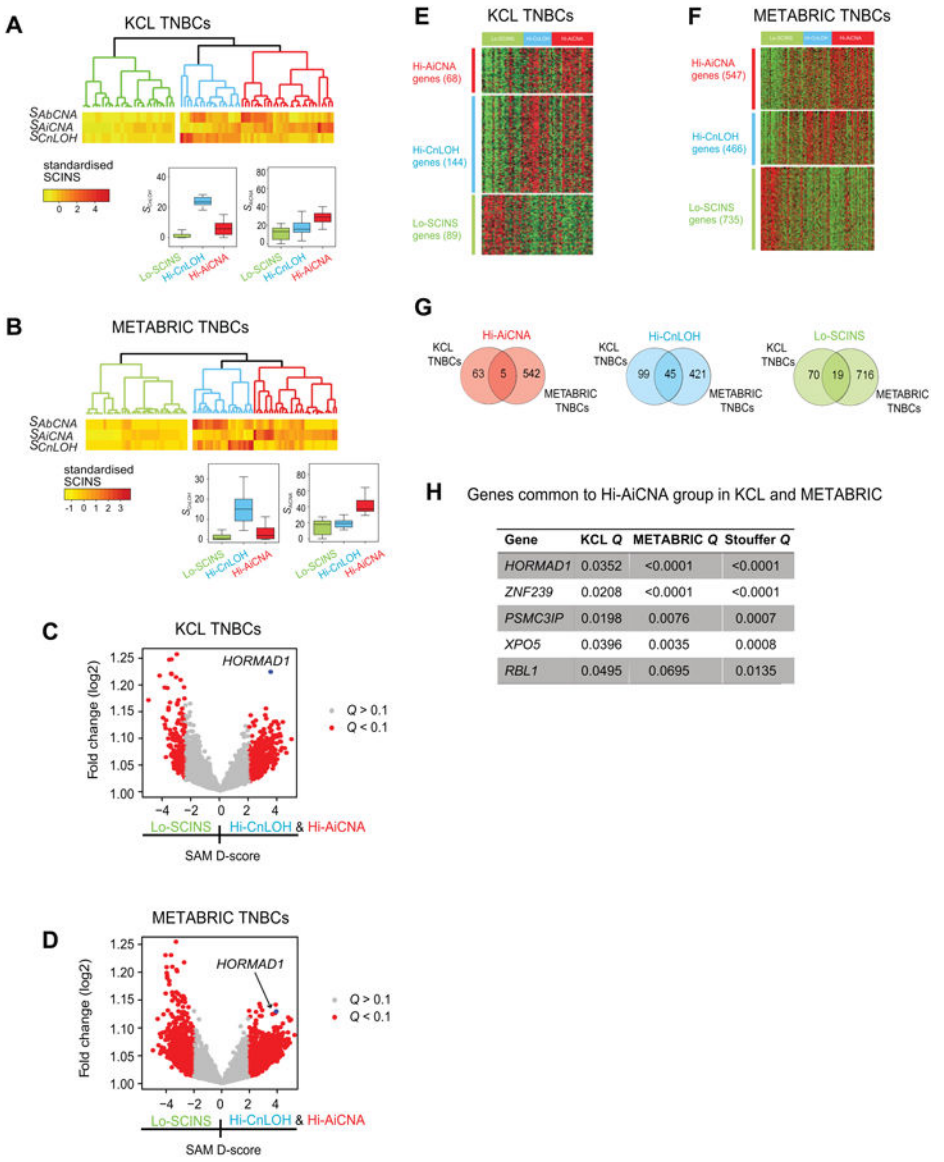

Gene	KCL Q	METABRIC Q	Stouffer Q
HORMAD1	0.0352	<0.0001	<0.0001
ZNF239	0.0208	<0.0001	<0.0001
PSMC3IP	0.0198	0.0076	0.0007
XPO5	0.0396	0.0035	0.0008
RBL1	0.0495	0.0695	0.0135

Figure 2. SCINS-defined tumour classes show distinct transcriptomic profiles

A and B, heatmaps (yellow-red image) and dendrograms showing the results of clustering 77 TNBCs from the KCL dataset (**A**) and 97 TNBCs from the METABRIC dataset (**B**), according to S_{AbCNA}, S_{AiCNA} and S_{CnLOH}. The three TNBC clusters identified for each dataset include Lo-SCINS (green arm of dendrogram), Hi-AiCNA (red arm of dendogram) and Hi-CnLOH (blue arm of dendrogram). Scores were standardised by row mean and a colour scale is shown to the left of each heatmap. Labels for each SCINS measure are displayed on the left. Boxplots underneath depict the distribution of S_{AiCNA} and S_{CnLOH} across the three clusters, identifying for each dataset a Lo-SCINS (green arm of dendrogram), a Hi-AiCNA (red arm of dendogram) and a Hi-CnLOH (blue arm of dendrogram) group. **C** and **D**, volcano plots of the $\log_2$ fold change of expression for all genes against the SAM D-score for the KCL (**C**) and METABRIC (**D**) datasets. Positive D-scores indicate an association to the composite Hi-AiCNA/Hi-CnLOH cluster, whereas

negative D-scores represent an association to the Lo-SCINS cluster. Genes that were significantly associated with either cluster (FDR $Q < 0.1$; SAM) are coloured red, whereas non-significant associations are in grey. *HORMAD1* is indicated in blue and with an arrow. **E** and **F**, heatmaps of the genes differentially expressed between each of the three SCINS-defined cluster for the KCL dataset (**E**) and the METABRIC dataset (**F**) (FDR $Q < 0.1$, SAM). Samples (columns) are ordered according to the clusters in the corresponding SCINS heatmap with the expression of individual genes (rows) across the dataset. Heatmap colours represent mean-centred $\log_2$ expression values. The genes in each heatmap are ordered from top to bottom by ascending q-value, and then by the descending *T*-statistic value of the SAM method. The top panel of heatmaps show the genes that are predominantly expressed in the Hi-AiCNA cluster. The middle panel of heatmaps show genes differentially upregulated in the Hi-CnLOH cluster while the bottom panel shows those specifically upregulated in the Lo-SCINS cluster. **G**, Venn diagrams showing the overlap between the differentially expressed genes (FDR $Q < 0.1$, SAM) from the KCL and METABRIC TNBC data for the Hi-AiCNA clusters (red shading), Hi-CnLOH clusters (blue shading) and the Lo-SCINS clusters (green shading). **H**, table showing the 5 genes belonging to the Hi-AiCNA list in both KCL and METABRIC, including *HORMAD1*.

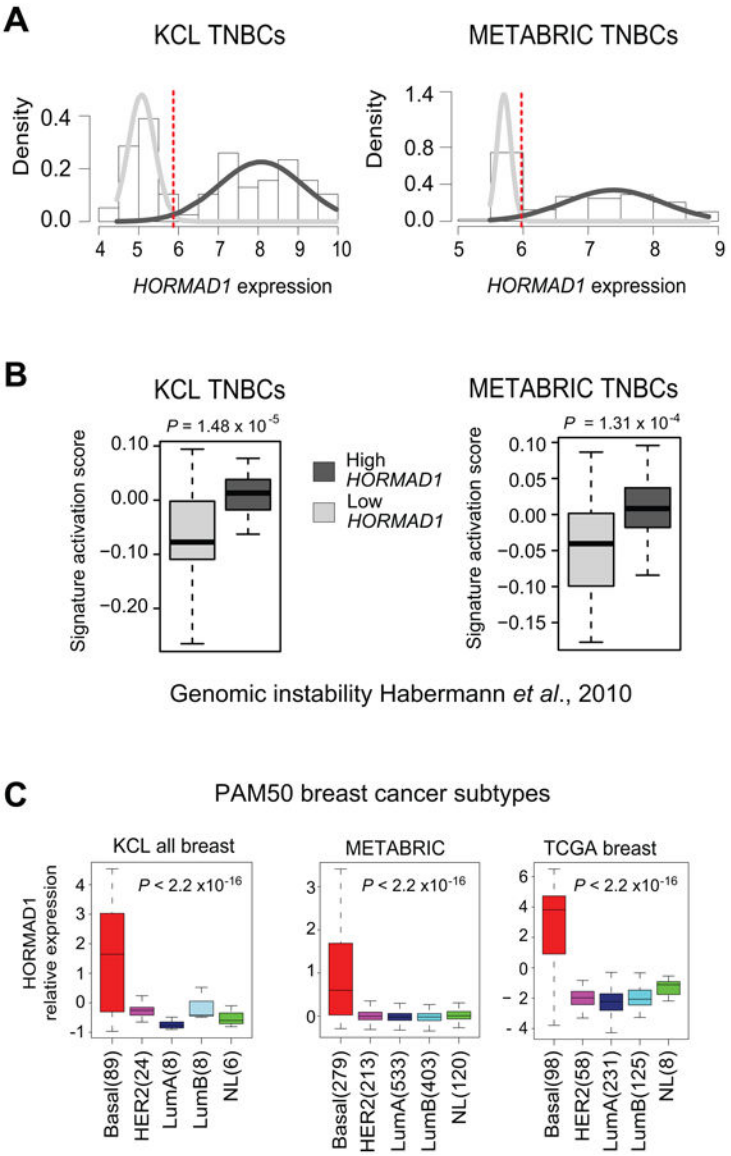

Figure 3. The distribution of *HORMAD1* expression in breast cancer

A, bimodal distributions of *HORMAD1* expression across the KCL (left) and METABRIC (right) TNBCs. Light and dark grey curves depict the distribution of low and high *HORMAD1*-expressing tumours, respectively. Maximum Likelihood Estimation was used to define the cut-off between high and low *HORMAD1* expressing tumours. **B**, box plots of the weighted, median-centred expression of genes (vertical axes) present in a previously published signature of high genomic instability (53). **C**, box plots showing the expression of *HORMAD1* across all breast cancer subtypes as classified by PAM50 in breast carcinomas enriched for TNBC from the KCL, the METABRIC and TCGA datasets.

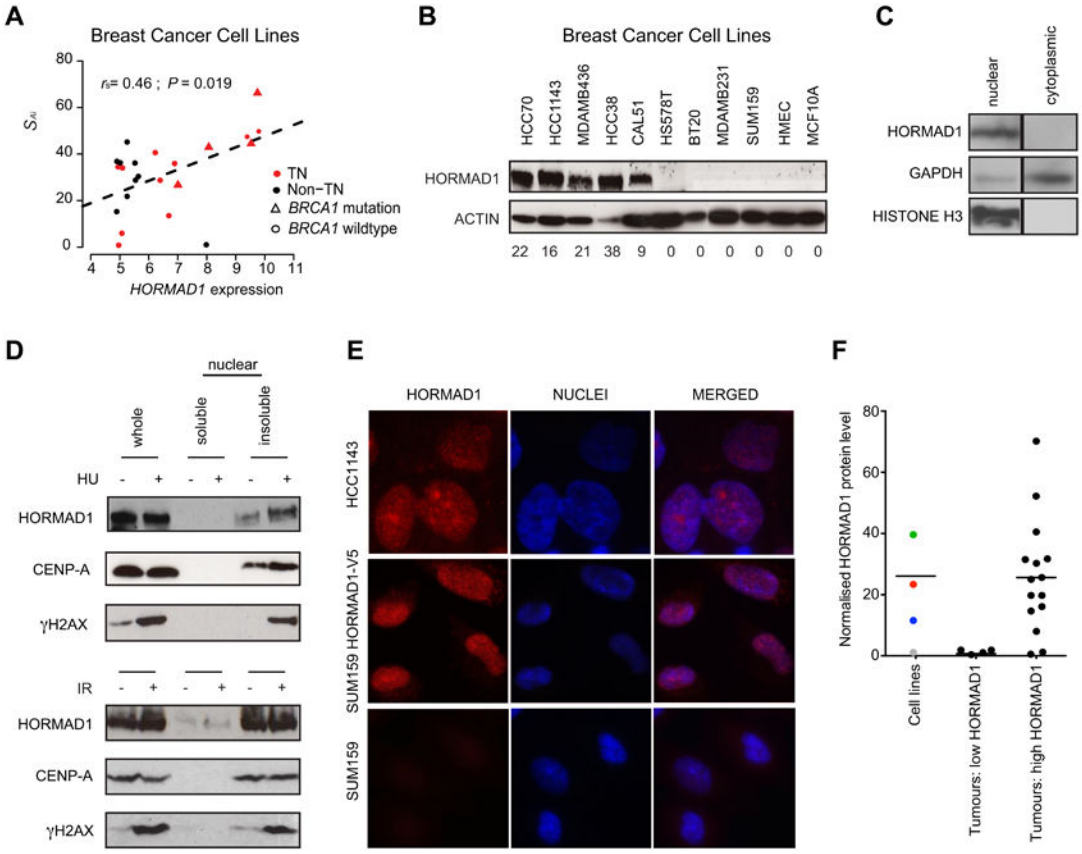

Figure 4. HORMAD1 expression in cell lines and primary tumour tissue

A, correlation of the composite S_{Ai} measure (vertical axis) with *HORMAD1* expression (horizontal axis) in 26 breast cell lines (red: TNBC; black: non-TNBC). *BRCA1* status of these samples is indicated by triangles (mutated) or circles (wildtype). Spearman's rank correlation coefficient and p-value are shown. **B**, western blot analysis of HORMAD1 in breast cancer and non-transformed cell lines, cell lysates were loaded in order of *HORMAD1* gene expression with highest expression being on the left. Values below blots represent quantification of HORMAD1 bands normalised to actin. **C,** subcellular fractionation of proteins in HCC1143 cells. **D**, Fractionation of nuclear proteins into nuclear soluble and insoluble fractions before and after DNA damage induction by Hydroxyurea (HU), top, and Irradiation (IR), bottom. Induction of DNA damage was validated by probing for γ-H2AX. **E,** immunofluorescence analysis of HORMAD1 localisation in breast cancer cell lines (red = HORMAD1, blue = nuclei). **F**, quantification of HORMAD1 protein levels by western blot in primary tumour samples and cell lines. Tumours are grouped into low and high HORMAD1 based on gene expression values using the bimodal cut-off value of 5.9. Cell lines are colour coded as follows: blue = HCC1143, red = SUM159-HORMAD1-V5, green = MDAMB436, grey = SUM159. In tumour samples, the central bar represents the mean protein level across all samples in that group, whereas in the cell lines, the mean of HORMAD1-positive samples only are shown.

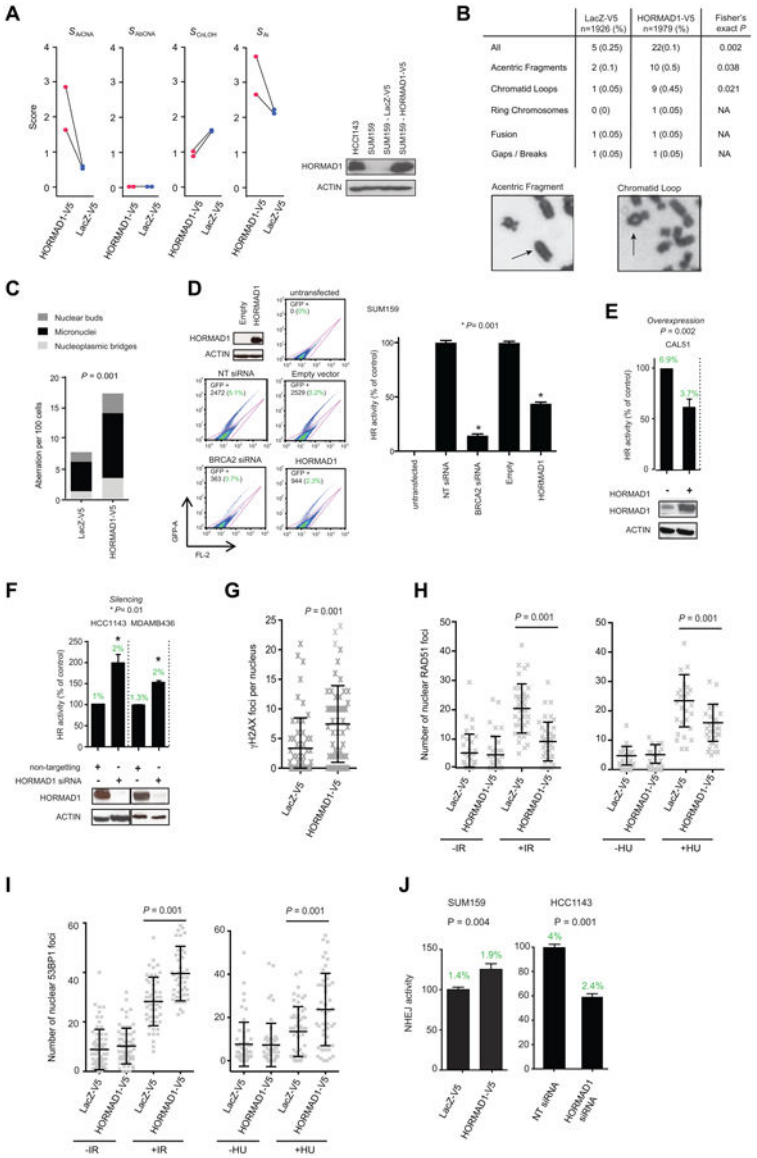

Figure 5. Overexpression of HORMAD1 induces the S_{AiCNA} scar, chromosome instability and changes in HR and NHEJ activity

A, plots showing the scores in two independent experiments to assess the level of the four SCINS measures following lentivirus-mediated expression of HORMAD1 (red) or LacZ control (blue) in the SUM159 cell line. Dots show the individual data points for a given cell line in an experiment. The lines pairing up the dots indicate the results from the same experiment. Western blots show the expression of HORMAD1 using a lentiviral expression vector in the HORMAD1-negative cell line SUM159. The HORMAD1-positive cell line, HCC1143, is included as a control. **B,** frequency of chromosomal aberrations, metaphase spreads from SUM159-LacZ-V5 or SUM159-HORMAD1-V5 cells (bottom) were assessed for structural chromosomal aberrations. Data points were derived from counting >30 metaphases per condition from two independent infections. **C**, HORMAD1 expression causes an increase in aberrant nuclear structures. Data is presented as the number of aberrations per 100 cells with >500 cells per condition assessed. Statistical significance of

the total number of aberrations between SUM159-LacZ-V5 and SUM159-HORMAD1-V5 was assessed by Fisher's test, $P < 0.0001$. **D**, the DR-GFP reporter vector was used to assess the effect of expression of HORMAD1 on DNA damage repair by HR in SUM159 breast cancer cells. HR activity was assessed by quantifying GFP-positive cells 72 hours after co-transfection of DR-GFP and pCBASce. FACS plots, left, are shown from a representative experiment with absolute numbers; the proportion of GFP-positive cells is also shown. BRCA2 siRNA was included as a positive control. Bar plots, right, represent the mean and standard error of the mean (SEM) of three independent experiments. Statistical significance was assessed by a Student's t-test. **E**, the effect of HORMAD1 overexpression on DR-GFP HR reporter activity in CAL51. HR activity was assessed by quantifying GFP-positive cells 72 hours after co-transfection of DR-GFP and pCBASce. Bar plots represent the mean and standard error of the mean (SEM) of three independent experiments. Statistical significance was assessed by a Student's t-test. The mean absolute percentages of GFP-positive cells in each condition are stated in green above the bars. **F**, the effect of HORMAD1 knockdown on DR-GFP HR reporter activity in the HORMAD1 expressing cell lines, HCC1143 and MDAMB436. HR activity was assessed by quantifying GFP-positive cells 72 hours after co-transfection of DR-GFP and pCBASce. Bar plots represent the mean and standard error of the mean (SEM) of three independent experiments. Statistical significance was assessed by a Student's t-test. The mean absolute percentage of GFP-positive cells in each condition are stated in green above bars. **G**, SUM159-LacZ-V5 and SUM159-HORMAD1-V5 cells were assessed for the presence of spontaneous nuclear γ-H2AX foci. Data shown is representative of triplicate experiments. Data points represent the number of γ-H2AX foci in individual nuclei and bars represent mean and standard deviation for each condition. Statistical significance of the mean number of foci between each group was assessed by a Student's t-test. **H**, IR (left) and HU (right)-induced RAD51 focus formation in SUM159-LacZ-V5 or SUM159-HORMAD1-V5 cells. Data shown is representative of triplicate experiments. Data points represent the number of RAD51 foci in individual nuclei and bars represent mean and standard deviation for each condition. Statistical significance of the mean number of foci between each group was assessed by Student's t-test. **I,** IR (left) and HU (right)-induced 53BP1 focus formation in SUM159-LacZ-V5 or SUM159-HORMAD1-V5 cells. Data points represent the number of 53BP1 foci in individual nuclei and bars represent mean and standard deviation for each condition. Statistical significance of the mean number of foci between each group was assessed by Student's t-test. **J**, The EJ5 NHEJ reporter vector was used to assess NHEJ activity in HORMAD1 stably expressing SUM159 (left) and HORMAD1 knockdown HCC1143 (right). NHEJ activity is presented as a percentage compared to the control. Bars represent the mean of 3 independent transfections.

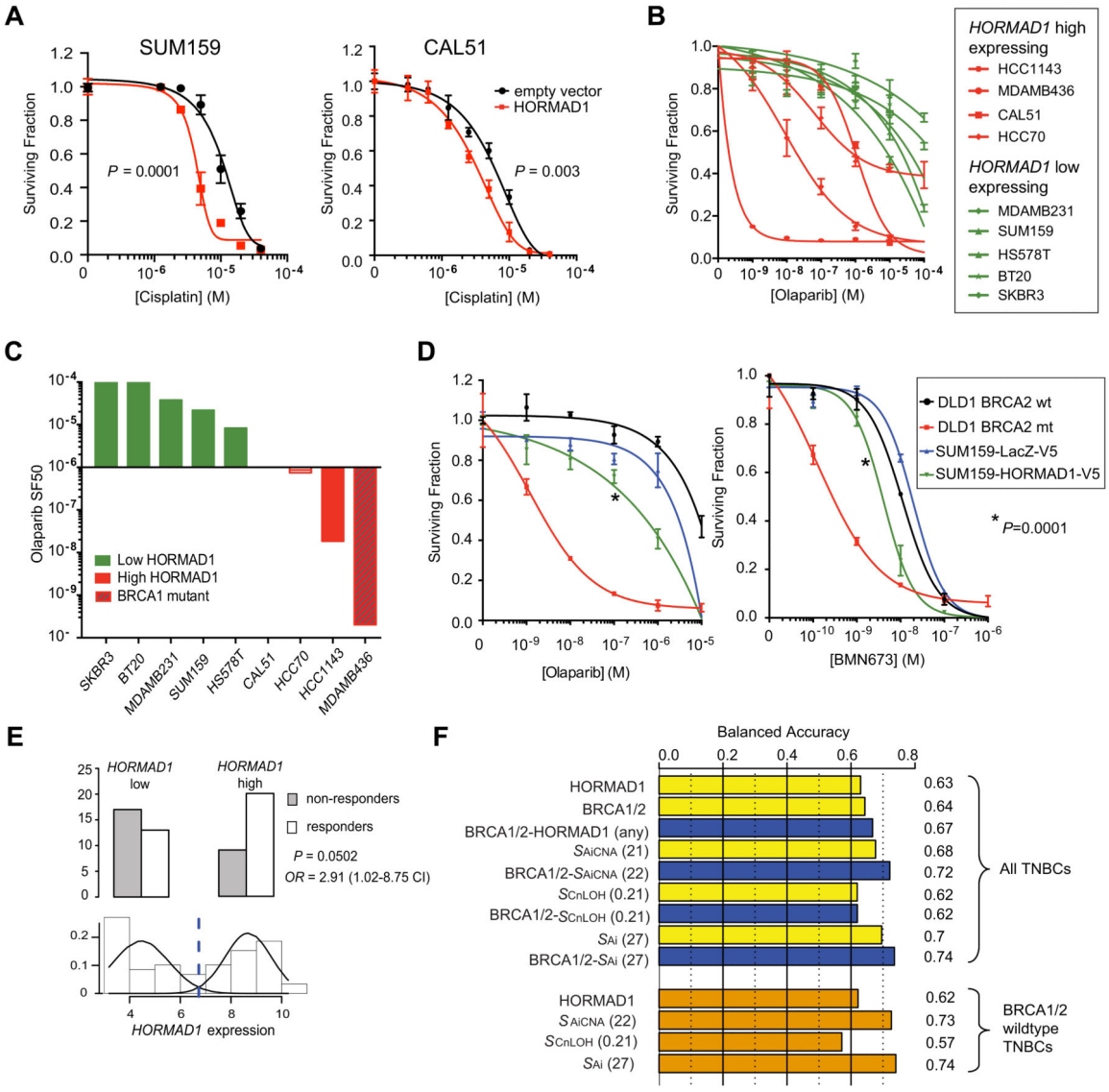

Figure 6. *HORMAD1* expression directly induces sensitivity, and contributes as an indicator of response to HR defect-targeting agents

A, cisplatin survival curves of SUM159 (left) and CAL51 (right) cells transfected with HORMAD1. Data shown are the mean and standard error of the mean from three experiments. Statistical significance was assessed using ANOVA. **B,** dose response olaparib survival curves for a panel of breast tumour cell lines. Cells were plated in six well plates and constantly exposed to olaparib for two weeks, at which point survival was estimated. As a control for olaparib sensitivity, the *BRCA1* null model MDAMB436 was used. Error bars represent standard error of the mean from three replica experiments. **C**, bar chart of olaparib SF50 values interpolated from survival curves. **D**, ectopic expression of *HORMAD1* drives PARP inhibitor sensitivity as shown by SUM159 cells expressing a HORMAD1-V5 fusion cDNA or a control LacZ cDNA, which were plated in 6 well plates and then exposed to either the clinical PARP inhibitor olaparib (left) or the clinical PARP inhibitor BMN673 (right). DLD1 BRCA2 wild type (wt) and mutant (mt) cells are included as a positive

control for PARP inhibitor sensitisation. Statistical significance was assessed using ANOVA. Error bars represent the standard error of the mean from three replica experiments. **E,** density curve (bottom) showing the distribution of *HORMAD1* expression in low (left of the dotted blue line) and high (right of the dotted blue line) *HORMAD1*-expressing PrECOG TNBCs. Above are the numbers of responders (white) and non-responders (grey) in the high and low *HORMAD1* settings. The odds ratio, 95% confidence intervals and p-value were obtained from a logistic regression model using drug response as the outcome. **F**, balanced accuracy was calculated by dividing the sum of sensitivity and specificity by two. Cutoffs for dichotomising the allelic-imbalanced-based predictors are shown in parentheses and were defined from ROC analyses. In the case of the combined BRCA1/2-HORMAD1 marker, categorisation of tumours into those without *HORMAD1* expression and *BRCA1/2* mutation, and those with at least one of these gene dysregulations was optimally accurate. Individual and combined predictors of platinum-based chemotherapeutic response using the whole PrECOG TNBC dataset are shown in yellow and blue, respectively. ROC analyses using dichotomised *HORMAD1*, S_{AiCNA}, S_{CnLOH} and S_{Ai} as predictors were used in the *BRCA1/2* wildtype subpopulation of the PrECOG dataset (bars in orange), and balanced accuracy computed as before.

Figure 7. Mechanism of HORMAD1-induced genomic instability

A, HORMAD1 is an essential meiotic protein which plays at least four important roles in meiosis: it supports SPO11 to induce double strand breaks; acts alongside ATR as part of the meiotic silencing of unsynapsed chromosomes pathway; is essential for the formation of the synaptonemal complex and contributes to the maintenance of interhomolog bias in template choice for recombinational repair of double strand breaks. **B**, of these, its role in maintaining interhomolog bias is particularly relevant to its role in genomic instability in TNBC. HORMAD1 favours interhomolog repair by inhibiting RAD51 which functions in intersister chromatid repair, while promoting DMC1, an interhomlog-acting recombinase. This bias ensures chiasmata formation, which is essential for normal segregation of chromosomes at meiosis. When HORMAD1 is expressed out of context in mitotic cells this function of HORMAD1 induces genomic instability by inhibiting RAD51 activity and thus normal HR. This leads to an increased reliance on error-prone NHEJ resulting in aberrations including

AiCNA. Additionally, HORMAD1 may also promote non-conservative allelic or repetitive sequence driven homologous recombination.